



PUBLISHED FOR SISSA BY SPRINGER

RECEIVED: December 10, 2012

REVISED: April 4, 2013

ACCEPTED: April 20, 2013

PUBLISHED: May 15, 2013

Two-Higgs-doublet models and enhanced rates for a 125 GeV Higgs

Aleksandra Drozd,^{a,b} Bohdan Grzadkowski,^a John F. Gunion^b and Yun Jiang^b

^a*Department of Physics, University of Warsaw,
Hoza 69, 00-681 Warsaw, Poland*

^b*Department of Physics, University of California,
1 Shields Avenue, Davis, CA 95616, U.S.A.*

E-mail: aleksandra.drozd@fuw.edu.pl, bohdan.grzadkowski@fuw.edu.pl,
jfgunion@ucdavis.edu, yunjiang@ucdavis.edu

ABSTRACT: We examine the level of enhancement that can be achieved in the ZZ and $\gamma\gamma$ channels for a two-Higgs-doublet model Higgs boson (either the light h or the heavy H) with mass near 125 GeV after imposing all constraints from LEP data, B physics, precision electroweak data, vacuum stability, unitarity and perturbativity. The latter constraints restrict substantially the possibilities for enhancing the $gg \rightarrow h \rightarrow \gamma\gamma$ or $gg \rightarrow H \rightarrow \gamma\gamma$ signal relative to that for the SM Higgs, h_{SM} . Further, we find that a large enhancement of the $gg \rightarrow h \rightarrow \gamma\gamma$ or $gg \rightarrow H \rightarrow \gamma\gamma$ signal in Type II models is possible only if the $gg \rightarrow h \rightarrow ZZ$ or $gg \rightarrow H \rightarrow ZZ$ mode is even more enhanced, a situation disfavored by current data. In contrast, in the Type I model one can achieve enhanced rates in the $\gamma\gamma$ final state for the h while having the ZZ mode at or below the SM rate — the largest $[gg \rightarrow h \rightarrow \gamma\gamma]/[gg \rightarrow h_{\text{SM}}\gamma\gamma]$ ratio found is of order ~ 1.3 when the two Higgs doublet vacuum expectation ratio is $\tan\beta = 4$ or 20 and the charged Higgs boson has its minimal LEP-allowed value of $m_{H^\pm} = 90$ GeV.

KEYWORDS: Higgs Physics, Beyond Standard Model

ARXIV EPRINT: [1211.3580](https://arxiv.org/abs/1211.3580)

Contents

1	Introduction	1
2	2HDM models	1
3	Setup of the analysis	2
3.1	The $m_h = 125$ GeV or $m_H = 125$ GeV scenarios	5
3.2	$m_A = 125.1$ GeV and $m_h = 125$ GeV or $m_H = 125$ GeV scenario	16
3.3	$m_h = 125$ GeV and $m_H = 125.1$ GeV scenario	21
4	Conclusions	22

1 Introduction

The original data from the ATLAS and CMS collaborations [1, 2] provided an essentially 5σ signal for a Higgs-like resonance with mass of order 123–128 GeV. The updates from Moriond 2013 include those for the $\gamma\gamma$ channel from ATLAS [3] and CMS [4]. The earlier ATLAS and CMS gluon fusion induced rates were significantly enhanced relative to the Standard Model (SM) prediction. The Moriond ATLAS data still shows substantial enhancement for the $\gamma\gamma$ channel while the CMS MVA analysis finds a roughly SM-like rate in the $\gamma\gamma$ channel. Here, we consider the extent to which an enhanced $\gamma\gamma$ rate is possible in various 2HDM models once all relevant theoretical and experimental constraints are imposed.

It is known that enhancements with respect to the SM in the $\gamma\gamma$ channel are generically possible in two-Higgs-doublet models (2HDM) of Type-I and Type-II as explored in [6–10]. However, these papers do not make clear what level of enhancement is possible after all constraints from B physics and LEP data (B/LEP), precision electroweak data, unitarity and perturbativity are imposed. In this paper, we impose all such constraints and determine the maximum possible enhancement. We employ a full 1-loop amplitude for $\text{Higgs} \rightarrow \gamma\gamma$ without neglecting any contributions from possible states in the loop. We examine correlations with other channels. We also consider cases of degenerate scalar masses at ~ 125 GeV [11, 12].

2 2HDM models

The general Higgs sector potential employed is

$$\begin{aligned}
 \mathcal{V} = & m_{11}^2 \Phi_1^\dagger \Phi_1 + m_{22}^2 \Phi_2^\dagger \Phi_2 - \left[m_{12}^2 \Phi_1^\dagger \Phi_2 + \text{h.c.} \right] \\
 & + \frac{1}{2} \lambda_1 \left(\Phi_1^\dagger \Phi_1 \right)^2 + \frac{1}{2} \lambda_2 \left(\Phi_2^\dagger \Phi_2 \right)^2 + \lambda_3 \left(\Phi_1^\dagger \Phi_1 \right) \left(\Phi_2^\dagger \Phi_2 \right) + \lambda_4 \left(\Phi_1^\dagger \Phi_2 \right) \left(\Phi_2^\dagger \Phi_1 \right) \\
 & + \left\{ \frac{1}{2} \lambda_5 \left(\Phi_1^\dagger \Phi_2 \right)^2 + \left[\lambda_6 \left(\Phi_1^\dagger \Phi_1 \right) + \lambda_7 \left(\Phi_2^\dagger \Phi_2 \right) \right] \left(\Phi_1^\dagger \Phi_2 \right) + \text{h.c.} \right\},
 \end{aligned} \tag{2.1}$$

where, to avoid explicit \mathcal{CP} violation in the Higgs sector, all λ_i and m_{12}^2 are assumed to be real. We choose a basis in which

$$\langle \Phi_1 \rangle = \frac{v}{\sqrt{2}} \begin{pmatrix} 0 \\ \cos \beta \end{pmatrix} \quad \langle \Phi_2 \rangle = \frac{v}{\sqrt{2}} \begin{pmatrix} 0 \\ e^{i\xi} \sin \beta \end{pmatrix},$$

where $v = (\sqrt{2}G_F)^{-1/2} \approx 246$ GeV. By convention $0 \leq \beta \leq \pi/2$ is chosen. For real parameters, the phase ξ could still be non-zero if the vacuum breaks \mathcal{CP} spontaneously. We avoid parameter choices for which this happens and take $\xi = 0$. Then, we define

$$\Phi_a = \begin{pmatrix} \phi_a^+ \\ (v_a + \rho_a + i\eta_a)/\sqrt{2} \end{pmatrix} \quad a = 1, 2 \quad (2.2)$$

with $v_1 = v \cos \beta$ and $v_2 = v \sin \beta$. The neutral Goldstone boson is $G^0 = \eta_1 \cos \beta + \eta_2 \sin \beta$ while the physical pseudoscalar state is

$$A = -\eta_1 \sin \beta + \eta_2 \cos \beta. \quad (2.3)$$

The physical scalars are:

$$h = -\rho_1 \sin \alpha + \rho_2 \cos \alpha, \quad H = \rho_1 \cos \alpha + \rho_2 \sin \alpha. \quad (2.4)$$

Without loss of generality, one can assume that the mixing angle α varies between $-\pi/2$ and $\pi/2$. We choose our independent variables to be $\tan \beta$ and $\sin \alpha$, which are single valued in the allowed ranges.

We adopt the code 2HDMC [13, 14] for numerical calculations. All relevant contributions to loop induced processes are taken into account, in particular those with heavy quarks (t , b and c), W^\pm and H^\pm . A number of different input sets can be used in the 2HDMC context. We have chosen to use the “physical basis” in which the inputs are the physical Higgs masses (m_H, m_h, m_A, m_{H^\pm}), the vacuum expectation value ratio ($\tan \beta$), and the \mathcal{CP} -even Higgs mixing angle, α , supplemented by m_{12}^2 . The additional parameters λ_6 and λ_7 are assumed to be zero as a result of a Z_2 symmetry being imposed on the dim 4 operators under which $H_1 \rightarrow H_1$ and $H_2 \rightarrow -H_2$. $m_{12}^2 \neq 0$ is still allowed as a “soft” breaking of the Z_2 symmetry. With the above inputs, $\lambda_{1,2,3,4,5}$ as well as m_{11}^2 and m_{22}^2 are determined (the latter two via the minimization conditions for a minimum of the vacuum) [15].

In this paper we discuss the Type I and Type II 2HDM models, that are defined by the fermion coupling patterns as specified in table 1 — for more details see [16].

3 Setup of the analysis

The 2HDMC code implements precision electroweak constraints (denoted STU) and limits coming from requiring vacuum stability, unitarity and coupling-constant perturbativity (denoted jointly as SUP). We note that it is sufficient to consider the SUP constraints at tree level as usually done in the literature. Evolution to higher energies would make these constraints, outlined below, stronger and would not be appropriate when considering the 2HDM as an effective low energy theory. In more detail, the vacuum stability condition requires that the scalar potential be positive in all directions in the limit of growing field

	Type I			Type II		
Higgs	up quarks	down quarks	leptons	up quarks	down quarks	leptons
h	$\cos \alpha / \sin \beta$	$\cos \alpha / \sin \beta$	$\cos \alpha / \sin \beta$	$\cos \alpha / \sin \beta$	$-\sin \alpha / \cos \beta$	$-\sin \alpha / \cos \beta$
H	$\sin \alpha / \sin \beta$	$\sin \alpha / \sin \beta$	$\sin \alpha / \sin \beta$	$\sin \alpha / \sin \beta$	$\cos \alpha / \cos \beta$	$\cos \alpha / \cos \beta$
A	$\cot \beta$	$-\cot \beta$	$-\cot \beta$	$\cot \beta$	$\tan \beta$	$\tan \beta$

Table 1. Fermionic couplings $C_{ff}^{h_i}$ normalized to their SM values for the Type I and Type II two-Higgs-doublet models.

strength [17–19]. Tree-level necessary and sufficient conditions for unitarity are formulated in terms of eigenvalues of the S-matrix in the manner specified in [20] for the most general 2HDM — the criterion is that the multi-channel Higgs scattering matrix must have a largest eigenvalue below the unitarity limit. Coupling constant perturbativity is defined as in 2HDMC by the requirement that all self-couplings among the Higgs-boson mass eigenstates be smaller than 4π . For the scenarios we consider, this becomes an important constraint on λ_1 . The SUP constraints are particularly crucial in limiting the level of enhancement of the $gg \rightarrow h \rightarrow \gamma\gamma$ channel, which is our main focus. For all our scans, we have supplemented the 2HDMC code by including the B/LEP constraints. For the LEP data we adopt upper limits on $\sigma(e^+e^- \rightarrow Zh/H)$ and $\sigma(e^+e^- \rightarrow Ah/H)$ from [21] and [22], respectively.¹ Regarding B physics, the constraints imposed are those from $\text{BR}(B_s \rightarrow X_s\gamma)$, R_b , ΔM_{B_s} , ϵ_K , $\text{BR}(B^+ \rightarrow \tau^+\nu_\tau)$ and $\text{BR}(B^+ \rightarrow D\tau^+\nu_\tau)$. The most important implications of these results are to place a lower bound on m_{H^\pm} as a function of $\tan\beta$ as shown in figure 15 of [23] in the case of the Type II model and to place a lower bound on $\tan\beta$ as a function of m_{H^\pm} as shown in figure 18 of [23] in the case of the Type I model.

While looking for an enhancement of the signal in the $\gamma\gamma$ channel we also computed the extra Higgs-sector contributions to the anomalous magnetic moment of the muon, $a_\mu = (g_\mu - 2)/2$. Since the experimentally measured value, $a_\mu = (1165920.80 \pm 0.63) \times 10^{-9}$ [24], differs by $\sim 3\sigma$ from its SM value it is important to check correlations between $\delta a_\mu \equiv a_\mu - a_\mu^{SM}$ and the signal in the $\gamma\gamma$ channel. Given the B/LEP, STU and SUP constraints, it turns out that one-loop contributions within the 2HDM are small and negligible, and the leading contribution is that known as the Barr-Zee diagram [25] which emerges at the two-loop level. For completeness we include also sub-leading contributions, see [13, 14]. Since the overall $\sim 3\sigma$ discrepancy between the experimental and theoretical SM values could still be due to fluctuations (the world average is based mainly on the E821 result [26] with uncertainties dominated by statistics) or underestimates of the theoretical uncertainties, we do not use the a_μ measurement as an experimental constraint on the models we discuss. However, in tables presented hereafter we do show (in the very last column in units of 10^{-11}) δa_μ , the judgment as to whether δa_μ is acceptable being left to the reader. In fact, for all parameter choices yielding an enhanced Higgs to two-photon rate the extra contributions to a_μ are very small and the a_μ discrepancy is not resolved.

¹We have modified the subroutine in 2HDMC that calculates the Higgs boson decays to $\gamma\gamma$ and also the part of the code relevant for QCD corrections to the $q\bar{q}$ final state.

	scenario I	scenario II	scenario III	scenario IV	scenario V
m_h [GeV]	125	{5,25,45,65,85,105,124.9}	125	125	{5,25,45,65,85,105,124.9}
m_H [GeV]	$125+m_{\text{list}}$	125	125.1	$125+m_{\text{list}}$	125
m_A [GeV]	m_{list}	m_{list}	m_{list}	125.1	125.1
m_{H^\pm} [GeV]	tan β -dependent minimum value consistent with B -physics and other constraints (see caption for details)				
tan β	{0.5, 0.9, 1.0, 1.2, 1.4, 1.6, 1.8, 2, 3, 4, 5, 7, 10, 15, 20, 30, 40}				
sin α	{-1, ..., 1} in steps of 0.1				
m_{12}^2 [GeV ²]	{ $\pm(1000)^2, \pm(750)^2, \pm(500)^2, \pm(400)^2, \pm(300)^2, \pm(200)^2, \pm(100)^2, \pm(50)^2, \pm(10)^2, \pm(0.1)^2$ }				

Table 2. Range of parameters adopted in the scans. In the table, m_{list} corresponds to the sequence of numbers $m_{\text{list}} = \{0.1, 10, 50, 100, 200, 300, 400, 500, 750, 1000\}$. The values of m_{H^\pm} are bounded from below by the constraints from B physics, see figure 15 and figure 18 of [23] for the Type II and Type I models, respectively. We have read off the lower m_{H^\pm} bound values at each of the scanned tan β values from these figures. Aside from a few preliminary scans, we fix m_{H^\pm} at this minimum value while scanning in other parameters. This is appropriate when searching for the maximum $\gamma\gamma$ rate since the charged Higgs loop is largest for the smallest possible m_{H^\pm} .

For an individual Higgs, denoted h_i (where $h_i = h, H, A$ are the choices) we compute the ratio of the gg or WW -fusion (VBF) induced Higgs cross section times the Higgs branching ratio to a given final state, X , relative to the corresponding value for the SM Higgs boson as follows:

$$R_{gg}^{h_i}(X) \equiv (C_{gg}^{h_i})^2 \frac{\text{BR}(h_i \rightarrow X)}{\text{BR}(h_{\text{SM}} \rightarrow X)}, \quad R_{\text{VBF}}^{h_i}(X) \equiv (C_{WW}^{h_i})^2 \frac{\text{BR}(h_i \rightarrow X)}{\text{BR}(h_{\text{SM}} \rightarrow X)}, \quad (3.1)$$

where h_{SM} is the SM Higgs boson with $m_{h_{\text{SM}}} = m_{h_i}$ and $C_{gg}^{h_i}, C_{WW}^{h_i}$ are the ratios of the $gg \rightarrow h_i, WW \rightarrow h_i$ couplings (C_{WW}^A being zero at tree level) to those for the SM, respectively. Note that the corresponding ratio for $V^* \rightarrow Vh_i$ ($V = W, Z$) with $h_i \rightarrow X$ is equal to $R_{\text{VBF}}^{h_i}(X)$, given that kinematic factors cancel out of all these ratios and that these ratios are computed in a self-consistent manner (that is, treating radiative corrections for the SM Higgs boson in the same manner as for the 2HDM Higgs bosons). When considering cases where more than one h_i has mass of ~ 125 GeV [11], we sum the different R^{h_i} for the production/decay channel of interest. This is justified by the fact that we always choose masses (as indicated in table 2) that are separated by at least 100 MeV — in this case interference effects are negligible (given that the Higgs widths are substantially smaller than 100 MeV in the range of Higgs masses we consider).

We have performed five scans over the parameter space with the range of variation specified in table 2. In subsequent tables, if a tan β value is omitted it means that, for the minimum m_{H^\pm} value allowed according to the plots of ref. [23], no choice for the other parameters could be found for which all the B -physics, STU and SUP constraints could be satisfied.

3.1 The $m_h = 125$ GeV or $m_H = 125$ GeV scenarios

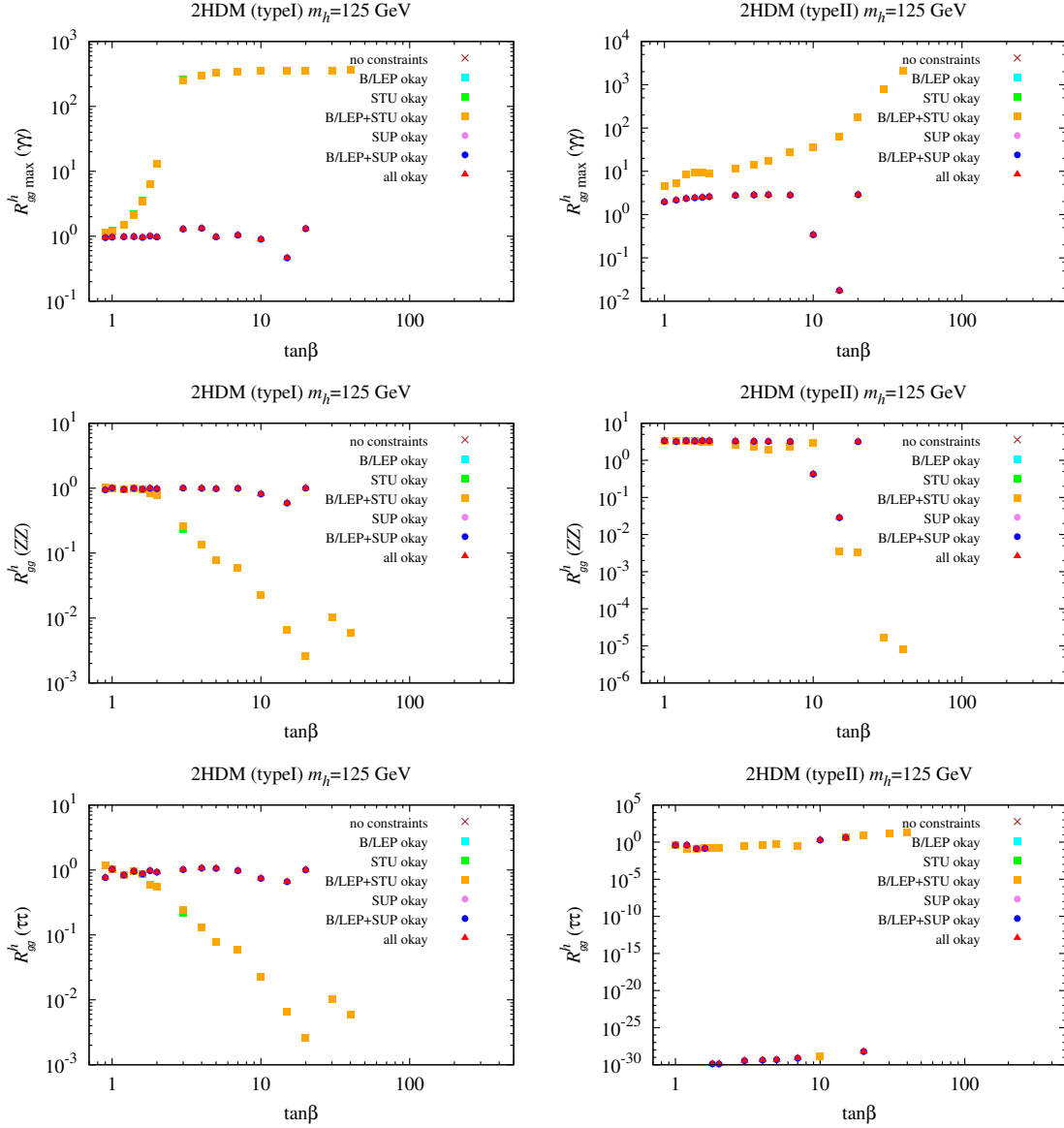


Figure 1. The top two plots show the maximum $R_{gg}^h(\gamma\gamma)$ values in the Type I (left) and Type II (right) models for $m_h = 125$ GeV as a function of $\tan\beta$ after imposing various constraints — see figure legend. Corresponding $R_{gg}^h(ZZ)$ and $R_{gg}^h(\tau\tau)$ are shown in the middle and lower panels. Disappearance of a point after imposing a given constraint set means that the point did not satisfy that set of constraints. In the case of boxes and circles, if a given point satisfies subsequent constraints then the resulting color is chosen according to the color ordering shown in the legend. This same pattern is adopted in the remaining plots.

$\tan \beta$	$R_{gg\max}^h(\gamma\gamma)$	$R_{gg}^h(ZZ)$	$R_{gg}^h(\tau\tau)$	$R_{VBF}^h(\gamma\gamma)$	$R_{VBF}^h(ZZ)$	$R_{VH}^h(b\bar{b})$	m_H	m_A	m_{H^\pm}	m_{12}	$\sin \alpha$	$\mathcal{A}_{H^\pm}^h/\mathcal{A}$	δa_μ
0.9	0.95	0.94	0.76	1.17	1.16	0.94	875	750	900	500	-0.8	-0.02	-2.1
1.0	0.97	1.00	1.02	0.95	0.98	1.00	875	750	850	500	-0.7	-0.02	-2.3
1.2	0.98	0.96	0.83	1.13	1.10	0.96	625	750	612	400	-0.7	-0.01	-2.0
1.4	0.99	0.99	0.96	1.02	1.03	0.99	525	750	460	300	-0.6	-0.01	-2.0
1.6	0.96	0.97	0.87	1.07	1.08	0.97	625	400	360	200	-0.6	-0.02	-1.9
1.8	1.01	1.00	0.98	1.03	1.01	1.00	425	400	285	200	-0.5	0.00	-2.0
2.0	0.98	0.98	0.92	1.04	1.04	0.98	425	500	350	200	-0.5	-0.01	-1.8
3.0	1.29	1.00	1.01	1.27	0.99	1.00	225	200	92	100	-0.3	0.12	-1.8
4.0	1.33	0.99	1.07	1.24	0.93	0.99	225	200	90	100	-0.1	0.14	-1.7
5.0	0.98	0.98	1.06	0.90	0.91	0.98	225	400	150	100	-0.0	0.01	-1.6
7.0	1.04	0.99	0.98	1.06	1.01	0.99	135	500	90	50	-0.2	0.02	-1.6
10.0	0.90	0.81	0.74	0.99	0.89	0.81	175	500	150	50	-0.5	0.04	-1.5
15.0	0.46	0.59	0.66	0.41	0.53	0.59	225	400	350	50	0.6	-0.11	-1.4
20.0	1.31	1.00	1.00	1.30	0.99	1.00	225	200	90	50	-0.0	0.13	-1.5

Table 3. Table of maximum $R_{gg}^h(\gamma\gamma)$ values for the Type I 2HDM with $m_h = 125$ GeV and associated R values for other initial and/or final states. The input parameters that give the maximal $R_{gg}^h(\gamma\gamma)$ value are also tabulated. $\tan \beta$ values, see table 2, for which the full set of constraints cannot be obeyed are omitted.

$\tan \beta$	$R_{gg\max}^h(\gamma\gamma)$	$R_{gg}^h(ZZ)$	$R_{gg}^h(\tau\tau)$	$R_{VBF}^h(\gamma\gamma)$	$R_{VBF}^h(ZZ)$	$R_{VH}^h(b\bar{b})$	m_H	m_A	m_{H^\pm}	m_{12}	$\sin \alpha$	$\mathcal{A}_{H^\pm}^h/\mathcal{A}$	δa_μ
0.5	1.56	2.69	1.84	0.52	0.89	0.61	425	500	600	100	-0.7	-0.06	-0.5
1.0	1.97	3.36	0.39	0.65	1.11	0.13	125	500	500	100	-0.2	-0.06	0.7
1.2	2.16	3.18	0.40	0.95	1.39	0.18	125	400	450	100	-0.2	-0.06	0.8
1.4	2.35	3.37	0.13	1.07	1.54	0.06	225	200	340	100	-0.1	-0.06	1.5
1.6	2.45	3.29	0.15	1.30	1.74	0.08	175	200	320	100	-0.1	-0.05	1.5
1.8	2.51	3.38	0.00	1.31	1.76	0.00	225	200	320	100	-0.0	-0.05	1.6
2.0	2.59	3.36	0.00	1.48	1.92	0.00	225	200	340	100	-0.0	-0.05	1.6
3.0	2.78	3.29	0.00	2.01	2.37	0.00	225	200	320	100	-0.0	-0.05	1.6
4.0	2.84	3.25	0.00	2.24	2.57	0.00	225	200	320	100	-0.0	-0.04	1.6
5.0	2.87	3.23	0.00	2.37	2.66	0.00	225	200	320	100	-0.0	-0.04	1.6
7.0	2.83	3.21	0.00	2.42	2.75	0.00	135	300	320	50	-0.0	-0.05	0.8
10.0	0.34	0.43	1.89	0.22	0.28	1.23	325	200	320	100	0.2	-0.08	3.5
15.0	0.02	0.03	4.06	0.00	0.01	0.87	225	200	320	50	0.6	-0.14	5.3
20.0	2.89	3.19	0.00	2.57	2.83	0.00	225	200	320	50	-0.0	-0.04	2.4

Table 4. Table of maximum $R_{gg}^h(\gamma\gamma)$ values for the Type II 2HDM with $m_h = 125$ GeV and associated R values for other initial and/or final states. The input parameters that give the maximal $R_{gg}^h(\gamma\gamma)$ value are also tabulated. $\tan \beta$ values, see table 2, for which the full set of constraints cannot be obeyed are omitted.

Let us begin by discussing the case in which the h has mass $m_h = 125$ GeV while scanning over the masses of the other Higgs eigenstates (cases where two Higgs are approximately degenerate are discussed below). The upper plots of figure 1 show the maximum value achieved for the ratio $R_{gg}^h(\gamma\gamma)$ as a function of $\tan\beta$ after scanning over all other input parameters (as specified earlier), in particular $\sin\alpha$. These maximum values are plotted both prior to imposing any constraints and after imposing various combinations of the constraints outlined earlier with point notation as specified in the figure legend. We observe that for most values of $\tan\beta$ the B/LEP and STU precision electroweak constraints, both individually and in combination, leave the maximum $R_{gg}^h(\gamma\gamma)$ unchanged relative to a full scan over all of parameter space. In contrast, the SUP constraints greatly reduce the maximum value of $R_{gg}^h(\gamma\gamma)$ that can be achieved and that value is left unchanged when B/LEP and STU constraints are imposed in addition. Remarkably, in the Type I model maximum $R_{gg}^h(\gamma\gamma)$ values much above 1.3 are not possible, with values close to 1 being more typical for most $\tan\beta$ values. In contrast, maximum $R_{gg}^h(\gamma\gamma)$ values in the range of 2–3 are possible for $2 \leq \tan\beta \leq 7$ and $\tan\beta = 20$ in the Type II model. In figure 1 we also show the values of $R_{gg}^h(ZZ)$ and $R_{gg}^h(\tau\tau)$ (middle and bottom plots, respectively) found for those parameter choices giving the maximum $R_{gg}^h(\gamma\gamma)$ values appearing in the upper plots.

One can get a feeling for how the different constraints impact $R_{gg}^h(\gamma\gamma)$ by plotting this quantity as a function of $\sin\alpha$ at fixed $\tan\beta$ for different constraint combinations and a selection of different other input parameters. As shown in figure 2, $R_{gg}^h(\gamma\gamma)$ typically has a maximum as $\sin\alpha$ is varied but the height of this maximum depends very much on the constraints imposed as there is also variation with the other input parameters.

Tables 3 and 4 display the full set of input parameters corresponding to the maximal $R_{gg}^h(\gamma\gamma)$ values at each $\tan\beta$ for models of Type I and Type II, respectively. It is important to notice that in the Type II model, the value of $R_{gg}^h(ZZ)$ corresponding to the parameters that maximize $R_{gg}^h(\gamma\gamma)$ is typically large, ~ 3 . In fact, as discussed shortly, $R_{gg}^h(ZZ) > R_{gg}^h(\gamma\gamma)$ whenever $R_{gg}^h(\gamma\gamma)$ is even modestly enhanced. The current experimental situation is confused. The Moriond 2013 ATLAS data [3] shows central values of $R_{gg}^h(\gamma\gamma) \sim 1.6$ and $R_{gg}^h(ZZ) \sim 1.5$. In the Type II model case, the former would imply $R_{gg}^h(ZZ) > 2$, somewhat inconsistent with the observed central value. However, the data uncertainties are significant and so it is too early to conclude that the Type II model cannot describe the ATLAS data. The Moriond 2013 CMS data has central values of $R_{gg}^h(\gamma\gamma) < 1$ and $R_{gg}^h(ZZ) \sim 1$, a situation completely consistent with the Type II model predictions.

As an aside, we note that $R_{gg}^h(\gamma\gamma)/R_{gg}^h(ZZ) \gtrsim 1$ when $R_{gg}^h(\gamma\gamma) > 1$ is fairly typical of the MSSM model (which has a Type II Higgs sector), especially with full or partial GUT scale unification for the soft-SUSY-breaking parameters, see for example [27]. In such scenarios the primary modification to the $\gamma\gamma$ rate relative to the SM is due to the light stop loop contribution to the $h\gamma\gamma$ coupling (which enters with the same sign as the W loop and has a color factor enhancement) which enhances $\text{BR}(h \rightarrow \gamma\gamma)$. Note that the stop loop contribution to the hgg production coupling is the same for both the ZZ and $\gamma\gamma$ final states. In the absence of GUT scale unification, there are many other potentially significant loops contributing to an increase in the $h\gamma\gamma$ coupling, the most important being the light chargino loop and the light stau loop, as studied for example in [28].

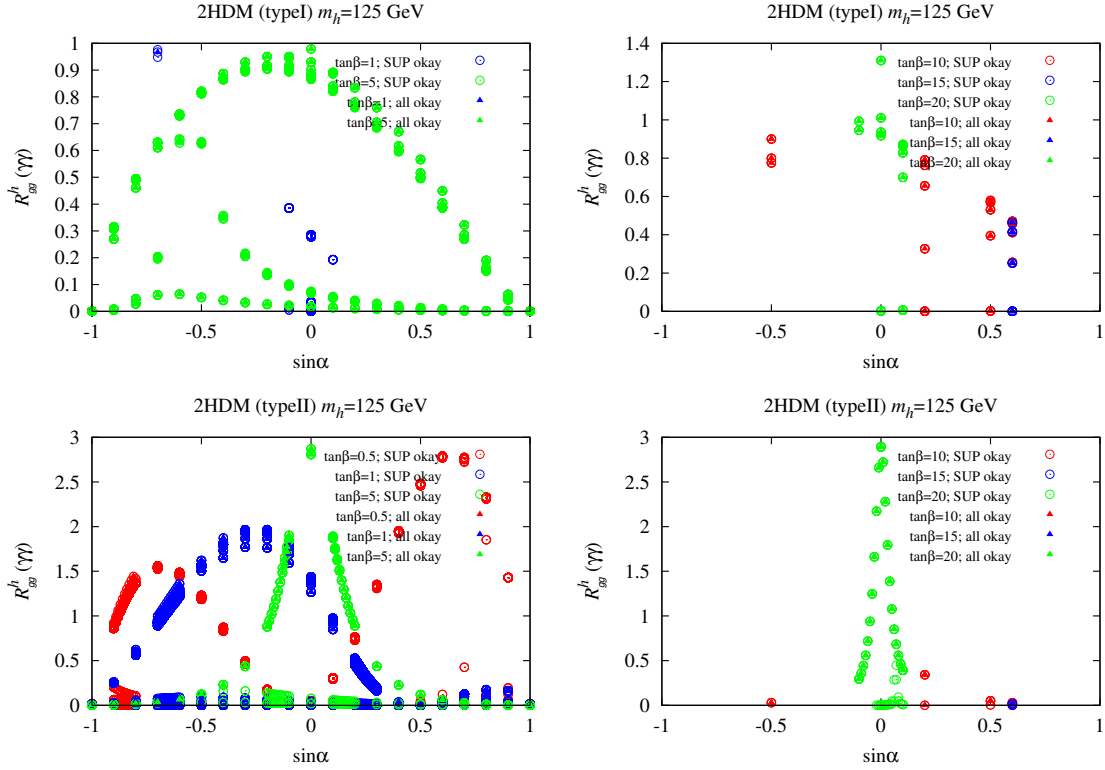


Figure 2. $R_{gg}^h(\gamma\gamma)$ is plotted for $m_h = 125$ GeV as a function of $\sin\alpha$ for a sequence of $\tan\beta$ values. Different constraint combinations are considered and the different curves of a given type correspond to a variety of other input parameters. The upper plots are for the Type I model and the lower plots are for the Type II model. Different colors indicate different $\tan\beta$ values. $\tan\beta$ values, see table 2, for which the full set of constraints cannot be obeyed are omitted.

$\tan \beta$	$R_{gg\max}^H(\gamma\gamma)$	$R_{gg}^H(ZZ)$	$R_{gg}^H(\tau\tau)$	$R_{\text{VBF}}^H(\gamma\gamma)$	$R_{\text{VBF}}^H(ZZ)$	$R_{VH}^H(b\bar{b})$	m_h	m_A	m_{H^\pm}	m_{12}	$\sin \alpha$	$\mathcal{A}_{H^\pm}^H/\mathcal{A}$	δa_μ
1.4	0.91	0.99	0.96	0.94	1.03	0.99	125	500	460	100	0.8	0.00	-2.7
1.6	0.89	0.97	0.87	1.00	1.08	0.97	125	400	360	50	0.8	0.00	-2.5
1.8	0.89	1.01	1.08	0.84	0.95	1.01	125	400	350	50	0.9	-0.06	-2.3
2.0	0.90	1.00	1.02	0.89	0.99	1.00	125	400	350	50	0.9	-0.05	-2.1
3.0	0.89	0.96	0.88	0.97	1.05	0.96	125	400	350	50	0.9	-0.05	-1.8
4.0	0.89	0.97	1.09	0.79	0.86	0.97	105	500	90	50	1.0	-0.03	-1.7
5.0	0.93	0.98	1.06	0.86	0.90	0.98	125	500	90	50	1.0	-0.01	-1.6
7.0	0.88	0.99	1.03	0.85	0.95	0.99	65	400	350	10	1.0	-0.05	-1.6
10.0	0.89	1.00	1.02	0.87	0.98	1.00	45	400	350	0	1.0	-0.05	-1.6
15.0	0.90	1.00	1.01	0.89	0.99	1.00	5	400	350	0	-1.0	-0.05	-1.6
20.0	0.90	1.00	1.00	0.89	0.99	1.00	25	400	350	0	-1.0	-0.05	-1.5
30.0	0.90	1.00	1.00	0.90	1.00	1.00	5	400	350	0	-1.0	-0.05	-1.5
40.0	0.90	1.00	1.00	0.90	1.00	1.00	5	400	350	0	-1.0	-0.05	-1.5

Table 5. Table of maximum $R_{gg}^H(\gamma\gamma)$ values for the Type I 2HDM with $m_H = 125$ GeV and associated R values for other initial and/or final states. The input parameters that give the maximal $R_{gg}^H(\gamma\gamma)$ value are also tabulated. $\tan \beta$ values, see table 2, for which the full set of constraints cannot be obeyed are omitted.

$\tan \beta$	$R_{gg}^H(\gamma\gamma)$	$R_{gg}^H(ZZ)$	$R_{gg}^H(\tau\tau)$	$R_{VBF}^H(\gamma\gamma)$	$R_{VBF}^H(ZZ)$	$R_{VH}^H(b\bar{b})$	m_h	m_A	m_{H^\pm}	m_{12}	$\sin \alpha$	$\mathcal{A}_{H^\pm}^H/\mathcal{A}$	δa_μ
1.0	1.99	3.24	0.52	0.71	1.16	0.19	125	500	500	100	1.0	-0.06	0.7
1.2	1.90	3.34	0.00	0.59	1.04	0.00	125	400	450	100	1.0	-0.06	0.8
1.4	2.20	3.38	0.00	0.86	1.32	0.00	125	300	340	100	1.0	-0.06	1.1
1.6	2.36	3.39	0.00	1.09	1.56	0.00	125	300	320	50	1.0	-0.06	1.1
1.8	2.48	3.38	0.00	1.29	1.76	0.00	125	300	320	50	1.0	-0.06	1.1
2.0	2.56	3.36	0.00	1.46	1.92	0.00	125	300	340	50	1.0	-0.06	1.1
3.0	2.73	3.29	0.00	1.97	2.37	0.00	125	300	320	50	1.0	-0.05	1.0
4.0	2.78	3.25	0.00	2.20	2.57	0.00	125	300	320	50	-1.0	-0.05	1.0
5.0	2.81	3.23	0.00	2.32	2.66	0.00	125	300	320	50	-1.0	-0.05	0.9
7.0	2.80	3.21	0.00	2.40	2.75	0.00	65	300	320	10	-1.0	-0.06	-0.0
10.0	2.81	3.20	0.00	2.46	2.79	0.00	45	300	320	0	-1.0	-0.06	-2.8
15.0	2.82	3.19	0.00	2.49	2.82	0.00	25	300	320	0	-1.0	-0.05	-16.9
20.0	2.82	3.19	0.00	2.50	2.83	0.00	25	300	320	0	-1.0	-0.05	-30.8
30.0	2.82	3.19	0.00	2.51	2.84	0.00	5	300	320	0	-1.0	-0.05	-38.7
40.0	2.82	3.19	0.00	2.51	2.84	0.00	5	300	320	0	-1.0	-0.05	-69.7

Table 6. Table of maximum $R_{gg}^H(\gamma\gamma)$ values for the Type II 2HDM with $m_H = 125$ GeV and associated R values for other initial and/or final states. The input parameters that give the maximal $R_{gg}^H(\gamma\gamma)$ value are also tabulated. $\tan \beta$ values, see table 2, for which the full set of constraints cannot be obeyed are omitted.

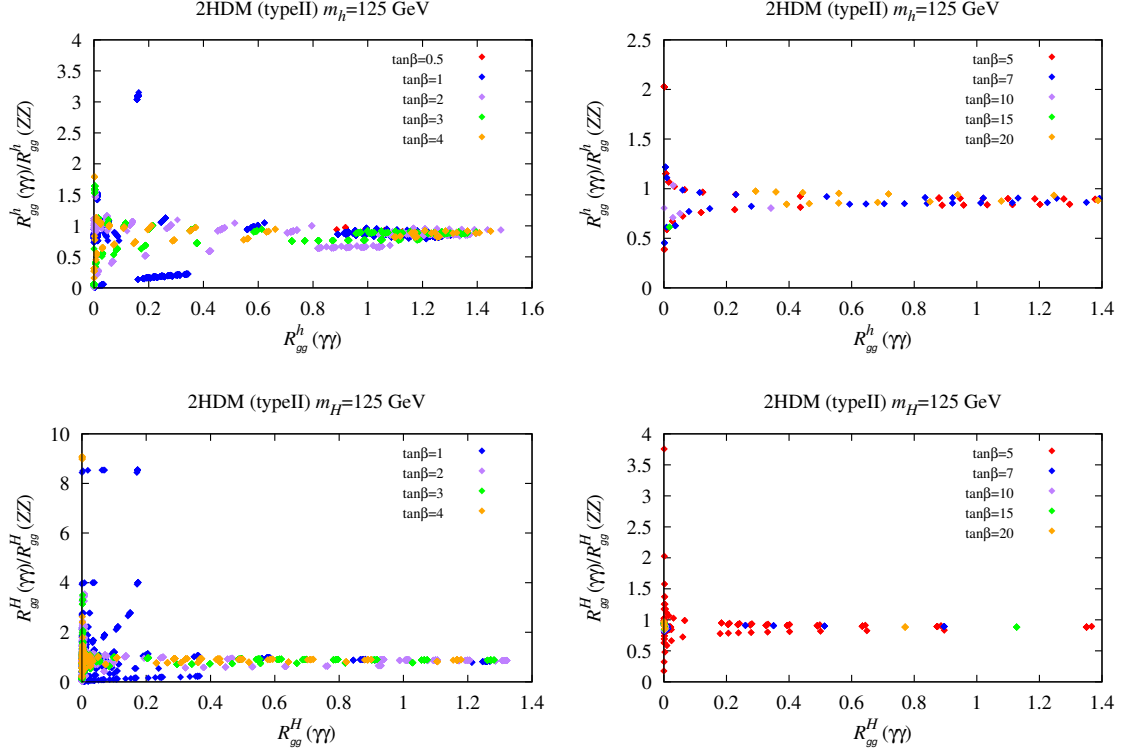


Figure 3. For the h (top) and H (bottom) we plot the gluon fusion induced $\gamma\gamma/ZZ$ ratio as a function of $R_{gg}(\gamma\gamma)$ for the Type II 2HDM.

Corresponding results for the H are presented for the Type I and Type II models in tables 5 and 6, respectively. In the case of the Type I model, an enhanced gluon fusion rate in the $\gamma\gamma$ final state does not seem to be possible after imposing the SUP constraints, whereas maximal enhancements of order $R_{gg}^H(\gamma\gamma) \sim 2.8$ are quite typical for the Type II model, albeit with even larger $R_{gg}^H(ZZ)$. Again, in the case of the Type II model $R_{gg}^H(\gamma\gamma)/R_{gg}^H(ZZ) < 1$ applies more generally whenever $R_{gg}^H(\gamma\gamma)$ is significantly enhanced.

That an enhanced $\gamma\gamma$ rate, e.g. $R_{gg}^{h,H}(\gamma\gamma) > 1.2$, leads to $R_{gg}^{h,H}(\gamma\gamma)/R_{gg}^{h,H}(ZZ) < 1$ in Type II models is illustrated by the plots of figure 3. We again emphasize that this is to be contrasted with the Type I model for which $R_{gg}^h(\gamma\gamma) > 1.2$ implies $R_{gg}^h(\gamma\gamma)/R_{gg}^{h,H}(ZZ) > 1$, see figure 4, in better agreement with current data. (For the Type I model, $R_{gg}^H(\gamma\gamma) > 1$ is not possible after imposing the SUP constraints.)

It is interesting to understand the mechanism behind the enhancement of $R_{gg}^{h,H}(ZZ)$ that seems to be an inevitable result within the Type II model if $R_{gg}^{h,H}(\gamma\gamma)$ is large. Let us define r as the ratio of $\gamma\gamma$ over ZZ production rates for a scalar s (either h or H). Then it is easy to see that

$$r_s \equiv \frac{R_{gg}^s(\gamma\gamma)}{R_{gg}^s(ZZ)} = \frac{\Gamma(s \rightarrow \gamma\gamma)/\Gamma(h_{sm} \rightarrow \gamma\gamma)}{\Gamma(s \rightarrow ZZ)/\Gamma(h_{sm} \rightarrow ZZ)}. \quad (3.2)$$

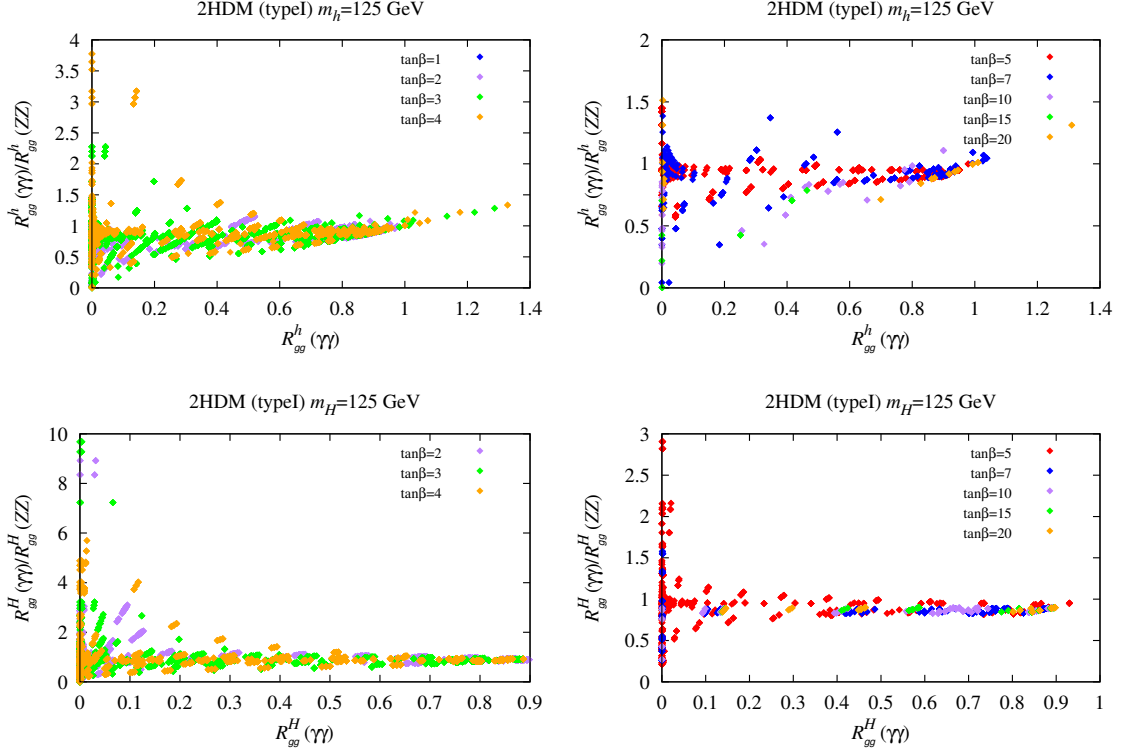


Figure 4. For the h (top) and H (bottom) we plot the gluon fusion induced $\gamma\gamma/ZZ$ ratio as a function of $R_{gg}(\gamma\gamma)$ for the Type I 2HDM.

For the decay mode $s \rightarrow ZZ^*$, the tree level amplitude is present and dominant so that the denominator simply reduces to $(C_{ZZ}^s)^2$. For the decay mode $s \rightarrow \gamma\gamma$, there is no tree level contribution — the $s\gamma\gamma$ coupling first arises at the one-loop level with the t -loop, W -loop and H^\pm -loop being the important contributions. As a result, the numerator can be written as

$$\frac{\Gamma(s \rightarrow \gamma\gamma)}{\Gamma(h_{sm} \rightarrow \gamma\gamma)} = \left(\frac{C_{WW}^s \mathcal{A}_W^{SM} - C_{t\bar{t}}^s \mathcal{A}_t^{SM} + \mathcal{A}_{H^\pm}}{\mathcal{A}_W^{SM} - \mathcal{A}_t^{SM}} \right)^2 \quad (3.3)$$

where $C_{t\bar{t}}^s$ and C_{WW}^s are the $st\bar{t}$ and sWW couplings normalized to those of the h_{SM} , while \mathcal{A}_W^{SM} and \mathcal{A}_t^{SM} are the W -loop and t -loop amplitudes, respectively, for the h_{SM} . Finally, \mathcal{A}_{H^\pm} is the H^\pm -loop amplitude in the 2HDM; since it is very small in the Type II model, it can be neglected. Thus,

$$r_s \simeq \frac{(C_{WW}^s)^2}{(C_{ZZ}^s)^2} \left(\frac{\mathcal{A}_W^{SM} - \frac{C_{t\bar{t}}^s}{C_{WW}^s} \mathcal{A}_t^{SM}}{\mathcal{A}_W^{SM} - \mathcal{A}_t^{SM}} \right)^2 = \left(\frac{\mathcal{A}_W^{SM} - \frac{C_{t\bar{t}}^s}{C_{WW}^s} \mathcal{A}_t^{SM}}{\mathcal{A}_W^{SM} - \mathcal{A}_t^{SM}} \right)^2 \quad (3.4)$$

where $C_{ZZ}^s = C_{WW}^s$ in any doublets+singlets models. Note that when the t -loop contribution is negligible then $r_s \rightarrow 1$. It is easy to see that $r_s < 1$ if the following inequality is

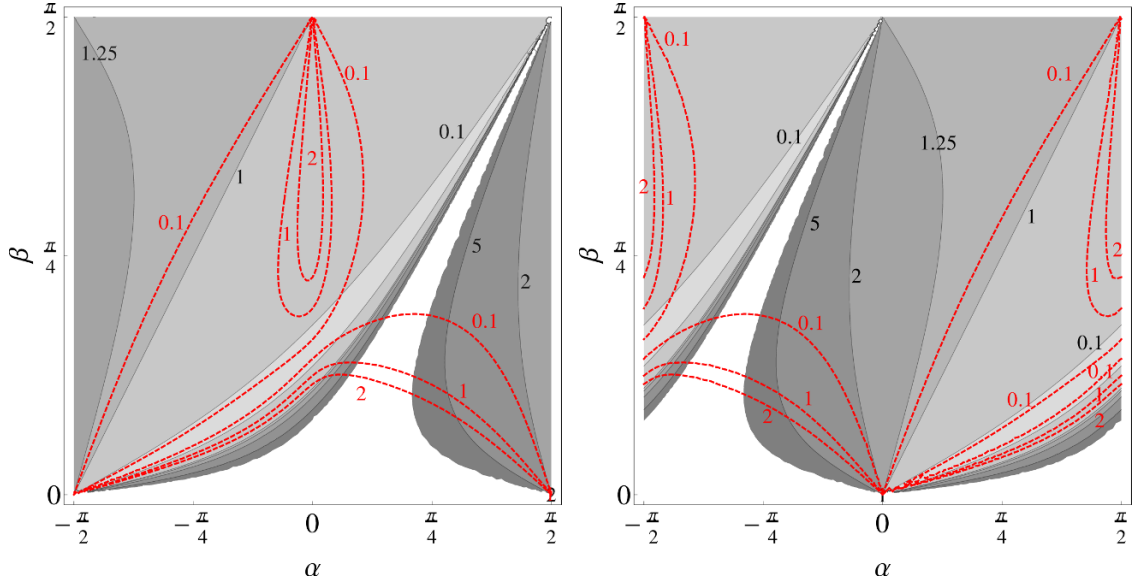


Figure 5. In the left panel we show contour plots (with shadowing) in the (β, α) space for r_h with superimposed red contours for $R_{gg}^h(\gamma\gamma)$. The right panel show similarly r_H with $R_{gg}^H(\gamma\gamma)$. Red numbers give constant values of $R_{gg}^h(\gamma\gamma)$ ($R_{gg}^H(\gamma\gamma)$) while black ones show constant values of r_h (r_H). The white region correspond to $r_s > 10.75$.

satisfied

$$1 < \frac{C_{t\bar{t}}^s}{C_{WW}^s} < 2 \frac{\mathcal{A}_W^{SM}}{\mathcal{A}_t^{SM}} - 1 \quad (3.5)$$

When $C_{t\bar{t}}^s/C_{WW}^s$ is outside of the above interval then $r_s > 1$. If s is the lighter scalar h then $C_{t\bar{t}}^s/C_{WW}^s = \cos \alpha / [\sin \beta \sin(\beta - \alpha)]$ implying $r_h < 1$ when

$$1 < \frac{\cos \alpha}{\sin \beta \sin(\beta - \alpha)} < 2 \frac{\mathcal{A}_W^{SM}}{\mathcal{A}_t^{SM}} - 1 \simeq 9, \quad (3.6)$$

while for $s = H$, $C_{t\bar{t}}^s/C_{WW}^s = \sin \alpha / [\sin \beta \cos(\beta - \alpha)]$ and we obtain $r_H < 1$ for

$$1 < \frac{\sin \alpha}{\sin \beta \cos(\beta - \alpha)} < 2 \frac{\mathcal{A}_W^{SM}}{\mathcal{A}_t^{SM}} - 1 \simeq 9. \quad (3.7)$$

In the case $s = h$, $R_{gg}^h(\gamma\gamma)$ is maximized by suppressing the h total width, which corresponds to choosing α so as to minimize the $hb\bar{b}$ coupling, i.e. $\alpha \sim 0$, resulting in $C_{t\bar{t}}^h/C_{WW}^h \sim 1/\sin^2 \beta > 1$ (and < 5 for $\tan \beta > 0.5$). Consequently $r_h < 1$, as observed in table 4. The argument is similar in the case of the H : this time the $Hb\bar{b}$ coupling is chosen to be small (equivalent to $\alpha \sim \pm\pi/2$) in order to minimize the H total width and therefore maximize $R_{gg}^H(\gamma\gamma)$, with the result that once again $C_{t\bar{t}}^H/C_{WW}^H \sim 1/\sin^2 \beta > 1$, yielding $r_H < 1$. These analytic results explain why large $R_{gg}^s(\gamma\gamma)$ is correlated with even larger $R_{gg}^s(ZZ)$ in Type II 2HDMs.

In figure 5 we plot contours of r_s and of $R_{gg}^s(\gamma\gamma)$ in the Type II model. It is seen from the left panel that if $\tan\beta$ is large then only small α 's will maximize $R_{gg}^s(\gamma\gamma)$. And, in that region, r_h is always less than 1. Note that the $R_{gg}^s(\gamma\gamma) > 1$ region shrinks for large $\tan\beta$, so the values of α preferred for large $R_{gg}^h(\gamma\gamma)$ converge to 0 when $\beta \rightarrow \pi/2$. For the case of $s = H$, the right panel shows that when $\tan\beta$ is large then only vertical bands of α corresponding to values close to $\pm\pi/2$ are allowed if $R_{gg}^s(\gamma\gamma) > 1$. From the plots, we see that $R_{gg}^s(\gamma\gamma) > 1$ could be consistent with $r_s > 1$ only if $\tan\beta \lesssim 1$, which explains the pattern observed in tables 4 and 6 and figure 3. Note, however, that small $\tan\beta$ is disfavored by B-physics as it enhances the $H^+\bar{t}b$ coupling too much, see for example [23].

Once again, we emphasize that a substantial enhancement of the $\gamma\gamma$ rate is possible for the h in Type I models without enhancing the ZZ rate. In particular, from table 3 we see that the enhancement in the $\gamma\gamma$ channel is ~ 1.3 (for both gg fusion and VBF) for $\tan\beta = 4$ and 20 while other final states, in particular ZZ , have close to SM rates. The table also shows that this maximum is achieved for $\sin\alpha \sim 0$. Thus, $\beta \sim \pi/2$ and $\cos\alpha \sim 1$ yielding SM-like coupling of the h to quarks (see table 1) and vector bosons. It turns out that in these cases the total enhancement, $\sim 30\%$, is provided by the charged Higgs boson loop contribution to the $\gamma\gamma$ -coupling. In these same cases, the mass of the heavier Higgs boson is $m_H = 225$ GeV. As such a mass is within the reach of the LHC, it is important to make sure that the H cannot be detected (at least with the current data set). It is easy to see that indeed this is the case. Since $g_{HZZ} \propto \cos(\beta - \alpha)$ and $g_{Hb\bar{b}, Ht\bar{t}} \propto \sin\alpha$ one finds that the H decouples from both vector bosons and fermions given that $\alpha \sim 0$ and $\beta \sim \pi/2$. The A will also be difficult to detect since it has no tree-level WW, ZZ coupling and the $A\bar{b}b, A\bar{t}t$ couplings, being proportional to $\cot\beta$, will be quite suppressed, especially at $\tan\beta = 20$. From table 3, we observe that for $\tan\beta = 4$ and 20 the corresponding charged Higgs is light, $m_{H^\pm} = 90$ GeV, i.e. as small as allowed by LEP2 direct searches in $e^+e^- \rightarrow H^+H^-$. Searches for a light H^\pm are underway at the LHC along the lines described in [29]. The most promising H^\pm production and decay process is $pp \rightarrow t\bar{t} \rightarrow H^\pm b W^\mp \bar{b} \rightarrow \tau \nu b \bar{b} q' \bar{q}$. According to figure 3 of [29], for the Type I model, the region of $\tan\beta \lesssim 6-7$ for $m_{H^\pm} \sim 90$ GeV could be efficiently explored at the 14 TeV LHC by ATLAS even at the integrated luminosity of 10 fb^{-1} — for more details see [29]. The existing LHC bounds on $BR(t \rightarrow H^+b)$ obtained assuming $BR(H^\pm \rightarrow \tau^\pm \nu_\tau) = 1$ are only moderately restrictive: $5\% - 1\%$ [30] ($4\% - 2\%$) [31] for masses of the charged Higgs boson $m_{H^\pm} = 90(80) - 160$ GeV in the case of ATLAS (CMS), respectively. These bounds are weakened in the Type I model where $BR(H^\pm \rightarrow \tau^\pm \nu_\tau) \simeq 0.7$. Since $BR(t \rightarrow H^+b) \sim 1/\tan^2\beta$, large $\tan\beta$ suppresses $BR(t \rightarrow H^+b)$. Indeed, it is easy to verify that for $m_{H^\pm} = 90$ GeV $BR(t \rightarrow H^+b)$ is $\sim 3.8\%$ and $\sim 0.15\%$ for $\tan\beta = 4$ and $\tan\beta = 20$, respectively. So, a charged Higgs yielding enhanced $h \rightarrow \gamma\gamma$ rates in gg fusion and VBF is still completely consistent with current data.

3.2 $m_A = 125.1$ GeV and $m_h = 125$ GeV or $m_H = 125$ GeV scenario

$\tan \beta$	$R_{gg\max}^{h+A}(\gamma\gamma)$	$R_{gg}^h(\gamma\gamma)$	$R_{gg}^A(\gamma\gamma)$	$R_{gg}^{h+A}(ZZ)$	$R_{gg}^{h+A}(\tau\tau)$	$R_{VBF}^h(\gamma\gamma)$	$R_{VBF}^h(ZZ)$	$R_{VH}^h(b\bar{b})$	m_H	m_{H^\pm}	m_{12}	$\sin \alpha$	$\mathcal{A}_{H^\pm}^b/\mathcal{A}$	δa_μ
1.2	1.31	0.90	0.41	1.02	3.35	0.83	0.94	1.02	625	612	100	-0.6	-0.05	-3.4
1.4	1.21	0.91	0.30	0.99	2.61	0.94	1.03	0.99	425	460	100	-0.6	-0.05	-2.9
1.6	1.14	0.91	0.23	1.01	2.32	0.87	0.97	1.01	425	360	100	-0.5	-0.05	-2.7
1.8	1.10	0.92	0.18	1.00	1.98	0.94	1.01	1.00	325	285	100	-0.5	-0.04	-2.4
2.0	1.08	0.93	0.15	0.98	1.73	0.99	1.04	0.98	325	230	100	-0.5	-0.04	-2.2
3.0	1.34	1.29	0.06	1.00	1.31	1.27	0.99	1.00	225	92	100	-0.3	0.12	-1.9
4.0	1.35	1.33	0.03	0.99	1.21	1.24	0.93	0.99	225	90	100	-0.1	0.14	-1.8
5.0	0.96	0.95	0.01	1.00	1.07	0.95	1.00	1.00	135	90	50	-0.2	-0.03	-1.7
7.0	1.04	1.04	0.01	0.99	1.00	1.06	1.01	0.99	135	90	50	-0.2	0.02	-1.6
10.0	0.91	0.90	0.01	0.81	0.77	0.99	0.89	0.81	175	150	50	-0.5	0.04	-1.5
15.0	0.42	0.42	0.00	0.59	0.67	0.37	0.53	0.59	225	250	50	0.6	-0.17	-1.4
20.0	1.31	1.31	0.00	1.00	1.00	1.30	0.99	1.00	225	90	50	-0.0	0.13	-1.6

Table 7. Table of maximum $R_{gg}^{h+A}(\gamma\gamma)$ values for the Type I 2HDM with $m_h = 125$ GeV, $m_A = 125.1$ GeV and associated R values for other initial and/or final states. The input parameters that give the maximal $R_{gg}^{h+A}(\gamma\gamma)$ value are also tabulated. Note that $R(b\bar{b})$ values can be obtained from this table by using $R(b\bar{b}) = R(\tau\tau)$. $\tan \beta$ values, see table 2, for which the full set of constraints cannot be obeyed are omitted.

The signal at 125 GeV cannot be pure A since the A does not couple to ZZ , a final state that is definitely present at 125 GeV. However, one can imagine that the \mathcal{CP} -even h or H and the A both have mass close to 125 GeV and that the net $\gamma\gamma$ rate gets substantial contributions from both the h or H and the A while only the former contributes to the ZZ rate. These possibilities are explored in figures 6 and 7, from which we observe that an enhanced $\gamma\gamma$ rate is only possible for the $m_h = 125, m_A = 125.1$ GeV choice. Details for this case appear in table 7.

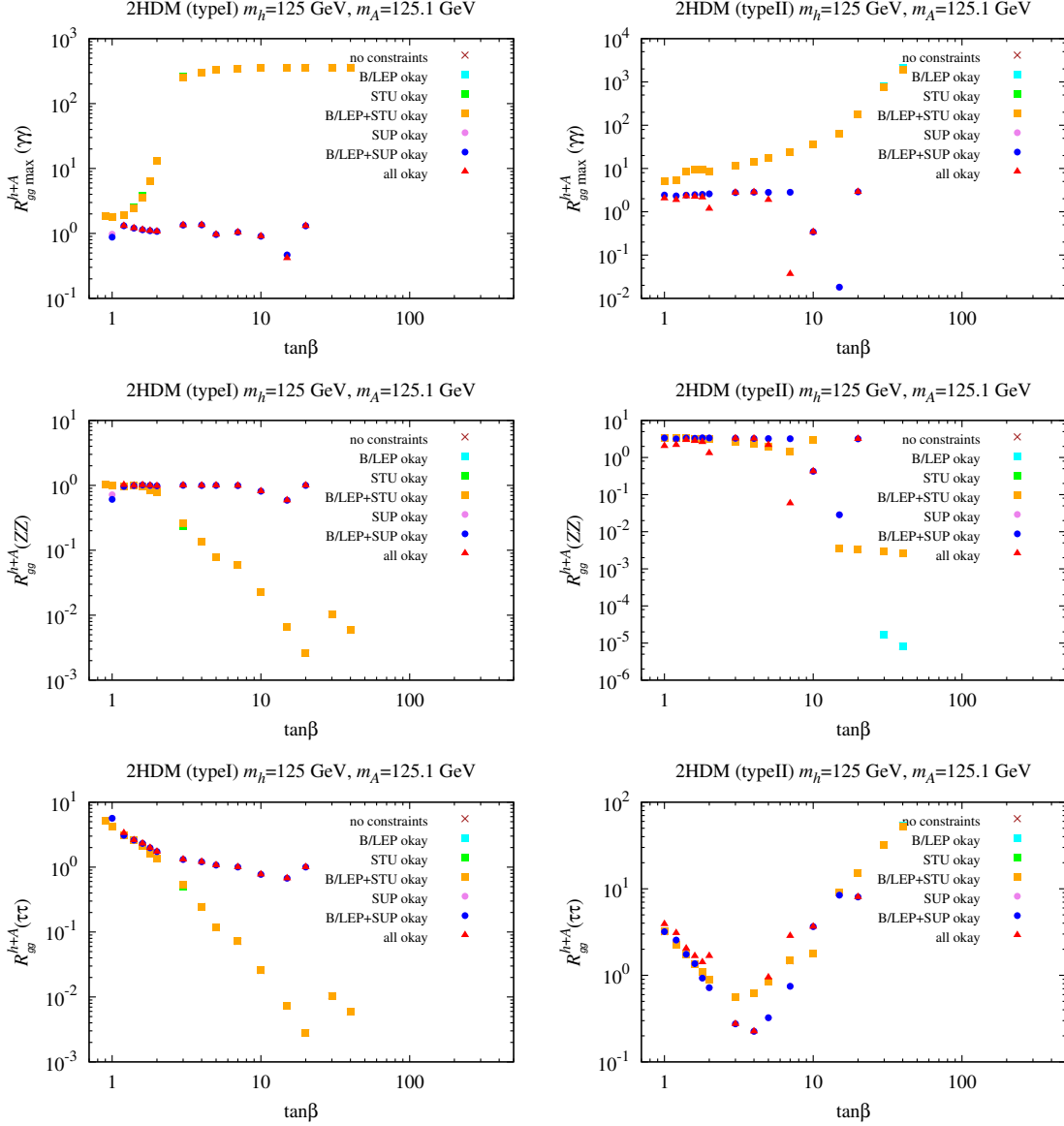


Figure 6. $R_{gg}^{h+A}(\gamma\gamma)$ maximum values when $m_h = 125$ GeV, $m_A = 125.1$ GeV as a function of $\tan\beta$ after imposing various constraints — see figure legend. Corresponding $R_{gg}^h(ZZ)$ and $R_{gg}^h(\tau\tau)$ ($= R_{gg}^h(b\bar{b})$) are shown in the middle and lower panels.

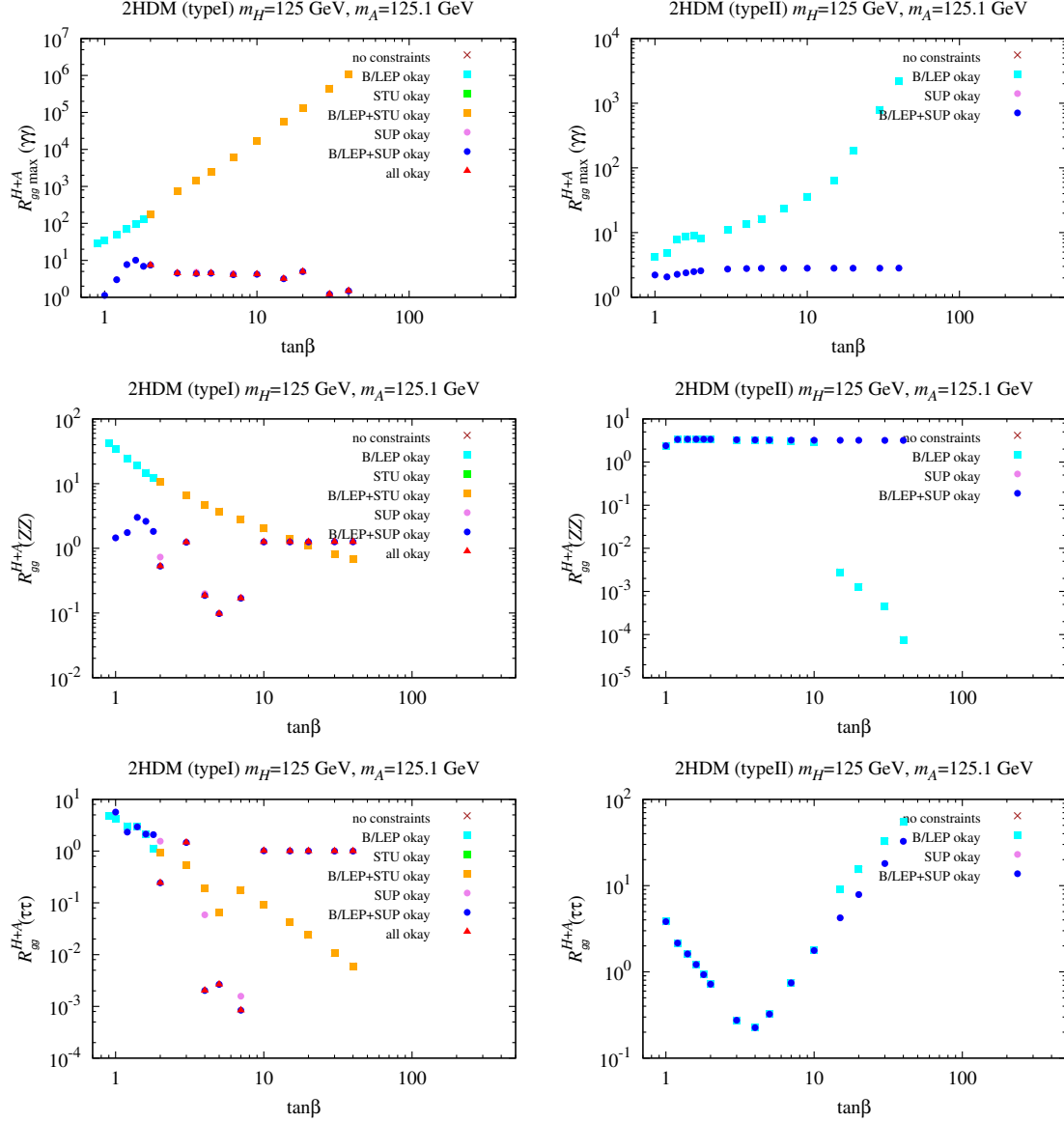


Figure 7. $R_{gg}^{h+A}(\gamma\gamma)$ maximum values when $m_H = 125$ GeV, $m_A = 125.1$ GeV as a function of $\tan\beta$ after imposing various constraints — see figure legend. Corresponding $R_{gg}^h(ZZ)$ and $R_{gg}^h(\tau\tau)$ ($= R_{gg}^h(b\bar{b})$) are shown in the middle and lower panels.

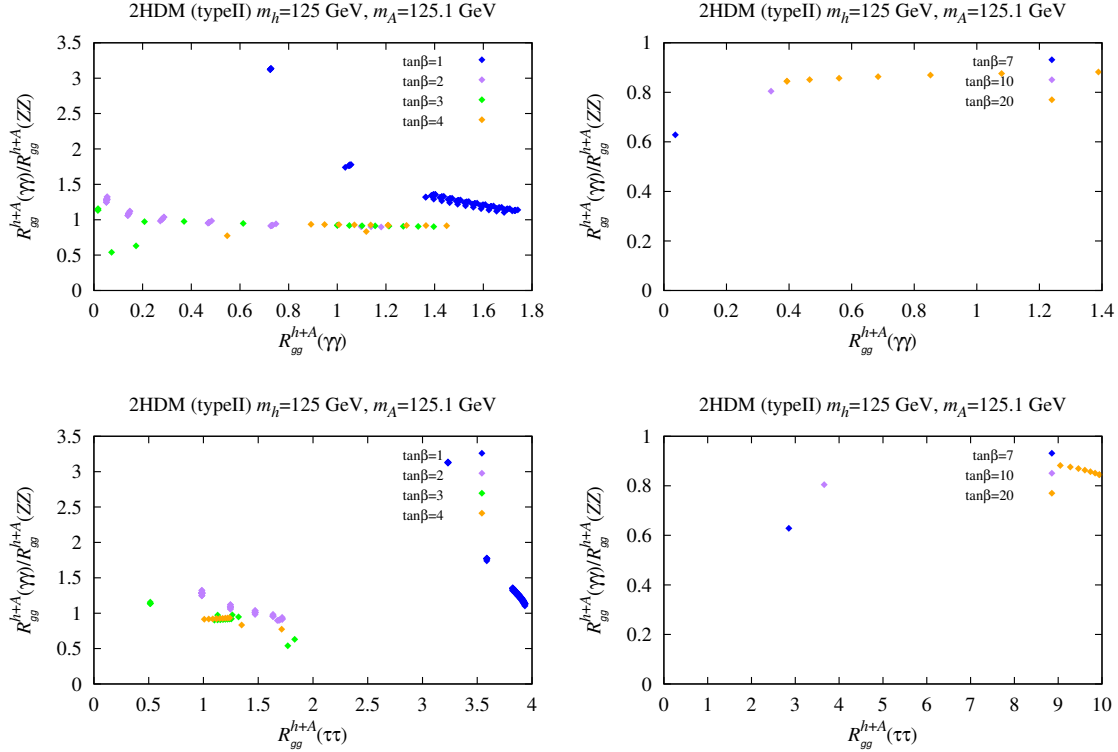


Figure 8. Correlations between $R_{gg}^{h+A}(\gamma\gamma)/R_{gg}^{h+A}(ZZ)$ and $R_{gg}^{h+A}(\gamma\gamma)$ (upper panels) and $R_{gg}^{h+A}(\gamma\gamma)/R_{gg}^{h+A}(\tau\tau)$ (lower panels) for selected values of $\tan\beta$.

For the Type I model, we see from table 7 that $R_{gg}^h(\gamma\gamma)$ is significantly enhanced only for the same $\tan\beta = 4$ and $\tan\beta = 20$ values as in the case of having (only) $m_h = 125$ GeV and that the pseudoscalar contribution $R_{gg}^A(\gamma\gamma)$ turns out to be tiny. However, the contribution to the $b\bar{b}$ final state from the A can be substantial. Given that the top loop dominates both the Agg and hgg coupling one finds $(C_{gg}^A/C_{gg}^h)^2 \sim (3/2)^2(\cos\beta/\cos\alpha)^2$, where we used $C_{tt}^A/C_{tt}^h = \cos\beta/\cos\alpha$ from table 1 and the $m_{h,A} \ll 2m_t$ fermionic loop ratio of $A/h = 3/2$. As a result, the A can contribute even more to the $b\bar{b}$ final state rate than the h if $\tan\beta$ is small. This (unwanted) contribution to the $b\bar{b}$ final state from A production is apparent from the results for $R_{gg}^{h+A}(b\bar{b})$ in table 7 for $\tan\beta = 2-4$. In the end, only $\tan\beta = 20$ yields both an enhanced $\gamma\gamma$ rate, $R_{gg\max}^{h+A}(\gamma\gamma) = 1.31$, and SM-like rates for the ZZ and $b\bar{b}$ final states, $R_{gg}^{h+A}(ZZ) = R_{gg}^{h+A}(b\bar{b}) = 1$. For this case $\beta \simeq \pi/2$ and $\alpha = 0$ implying that the h couples to fermions and gauge bosons like a SM Higgs boson and the enhancement of $R_{gg\max}^{h+A}(\gamma\gamma)$ is due exclusively to the charged Higgs loop contribution to the $\gamma\gamma$ couplings.

$\tan \beta$	$R_{gg\max}^{h+A}(\gamma\gamma)$	$R_{gg}^h(\gamma\gamma)$	$R_{gg}^A(\gamma\gamma)$	$R_{gg}^{h+A}(ZZ)$	$R_{gg}^{h+A}(\tau\tau)$	$R_{\text{VBF}}^h(\gamma\gamma)$	$R_{\text{VBF}}^h(ZZ)$	$R_{\text{VH}}^h(b\bar{b})$	m_H	m_{H^\pm}	m_{12}	$\sin \alpha$	$\mathcal{A}_{H^\pm}^h/\mathcal{A}$	δa_μ
1.0	2.05	1.58	0.47	2.05	3.91	0.93	1.22	0.65	525	500	100	-0.5	-0.06	1.3
1.2	1.88	1.71	0.17	2.19	3.08	1.05	1.34	0.57	425	450	100	-0.4	-0.05	1.5
1.4	2.29	2.22	0.07	2.99	2.04	1.18	1.59	0.23	325	340	100	-0.2	-0.05	1.9
1.6	2.23	2.20	0.03	2.80	1.67	1.34	1.71	0.28	225	320	100	-0.2	-0.05	2.0
1.8	2.15	2.14	0.01	2.63	1.42	1.44	1.77	0.33	225	320	100	-0.2	-0.05	2.0
2.0	1.18	1.17	0.01	1.31	1.68	1.07	1.20	0.87	325	340	100	-0.4	-0.05	1.5
3.0	2.78	2.78	0.00	3.29	0.27	2.01	2.37	0.00	225	320	100	-0.0	-0.05	2.3
4.0	2.84	2.84	0.00	3.25	0.23	2.24	2.57	0.00	225	320	100	-0.0	-0.04	2.3
5.0	1.89	1.89	0.00	2.19	0.95	1.41	1.64	0.47	225	320	100	0.1	-0.05	2.7
7.0	0.04	0.04	0.00	0.06	2.85	0.01	0.02	0.75	325	320	100	0.6	-0.15	5.2
10.0	0.34	0.34	0.00	0.43	3.66	0.22	0.28	1.23	325	320	100	0.2	-0.08	4.7
20.0	2.89	2.89	0.00	3.19	8.03	2.57	2.83	0.00	225	320	50	-0.0	-0.04	5.6

Table 8. Table of maximum $R_{gg}^{h+A}(\gamma\gamma)$ values for the Type II 2HDM with $m_h = 125$ GeV, $m_A = 125.1$ GeV and associated R values for other initial and/or final states. The input parameters that give the maximal $R_{gg}^{h+A}(\gamma\gamma)$ value are also tabulated. Note that $R(b\bar{b})$ values can be obtained from this table by using $R(b\bar{b}) = R(\tau\tau)$. $\tan \beta$ values, see table 2, for which the full set of constraints cannot be obeyed are omitted.

For the Type II model, see table 8, the pseudoscalar contribution $R_{gg}^A(\gamma\gamma)$ is also (as for the Type I model) negligible. Thus, the enhancement of $R_{gg}^{h+A}(\gamma\gamma)$ is essentially the same as that for $R_{gg}^h(\gamma\gamma)$ for the case when only $m_h = 125$ GeV, reaching maximum values of order 2–3. However, as in the pure $m_h = 125$ GeV case, a substantial enhancement of $R_{gg}^{h+A}(\gamma\gamma)$ is most often associated with $R_{gg}^{h+A}(ZZ) > R_{gg}^{h+A}(\gamma\gamma)$ (contrary to the LHC observations). But this is not *always* the case. Among the $m_h \sim m_A$ scenarios we find 56 points in our parameter space for which $R_{gg}^{h+A}(ZZ) < 1.3$ and $R_{gg}^{h+A}(\gamma\gamma) > 1.3$. Unfortunately for all those points the $\tau\tau$ signal is predicted to be too strong, $R_{gg}^{h+A}(\tau\tau) > 3.82$, a result that is now excluded by the CMS analysis in the gluon fusion dominated 1-jet trigger mode which finds $R_{gg}^{h+A}(\tau\tau) < 1.8$ at 95% CL. This situation is illustrated in figure 8. As seen from the upper panels in figure 8, for $\tan\beta = 1$ there exist points (blue diamonds) such that $\frac{R_{gg}^h(\gamma\gamma)}{R_{gg}^h(ZZ)} > 1$ and $R_{gg}^{h+A}(\gamma\gamma) > 1$ (or even > 1.5). However, the lower left panel of figure 8 shows that the $R_{gg}^{h+A}(\tau\tau)$ values that correspond to those points are greater than 3.5.

The case with $m_A \sim 125$ GeV and $m_H = 125$ GeV is less attractive. For the Type I model, the constraints are such that once parameters are chosen so that H and A have masses of 125 GeV and 125.1 GeV the maximum value achieved for $R_{gg}^{H+A}(\gamma\gamma)$ is rather modest reaching only 1.04 at small $\tan\beta$. For the Type II model, as seen in figure 7, there are no parameter choices for which the H and A have a mass of ~ 125 GeV while all other constraints are satisfied.

3.3 $m_h = 125$ GeV and $m_H = 125.1$ GeV scenario

Finally, we have the case where $m_h = 125$ GeV and $m_H = 125.1$ GeV and we allow m_{H^\pm} and m_A to vary freely. Following a similar search strategy, we find that some of the $\tan\beta$ values previously available when only $m_h = 125$ GeV or $m_H = 125$ GeV was required are ruled out by the full set of constraints and that there is no gain in maximal $R_{gg}^{h+H}(\gamma\gamma)$ values, and often some loss, relative to the cases where only the h or only the H was required to have mass of 125 GeV.

As discussed earlier and in [33], the charged Higgs contribution to the $\gamma\gamma$ coupling loops is sometimes relevant. Therefore, in figure 9 we show separately the fermionic loop, W loop and H^\pm loop contributions normalized to the total amplitude for the most interesting cases of a Type I model with $m_h = 125$ GeV and with $m_h = 125$ GeV, $m_A = 125.1$ GeV (left plots). One sees that the $\tan\beta$ values of 4 and 20 associated with $R_{gg}^h(\gamma\gamma) \sim 1.3$ are associated with large A_{H^\pm}/A . Indeed, in these two cases, the relative charged Higgs contribution reaches nearly ~ 0.2 and is as large as the fermionic contribution, but of the opposite sign. In fact, although the dominant loop is the W loop, the H^\pm loop may contribute as much as the dominant (top quark) fermionic loop.

This should be contrasted with other cases, such as the Type II $m_h = 125$ GeV and $m_h = 125$ GeV, $m_A = 125.1$ GeV cases illustrated in the right-hand plots of figure 9. One finds that the charged Higgs contributions are small when SUP constraints are imposed. In fact, the enhancement of $R_{gg}^h(\gamma\gamma)$ observed in figure 1 prior to imposing SUP is caused just by the charged Higgs loop. When SUP constraints are imposed the charged Higgs amplitude is strongly reduced by the requirement that the quartic couplings not violate the perturbativity condition. Note that the SUP constraints can be violated even though

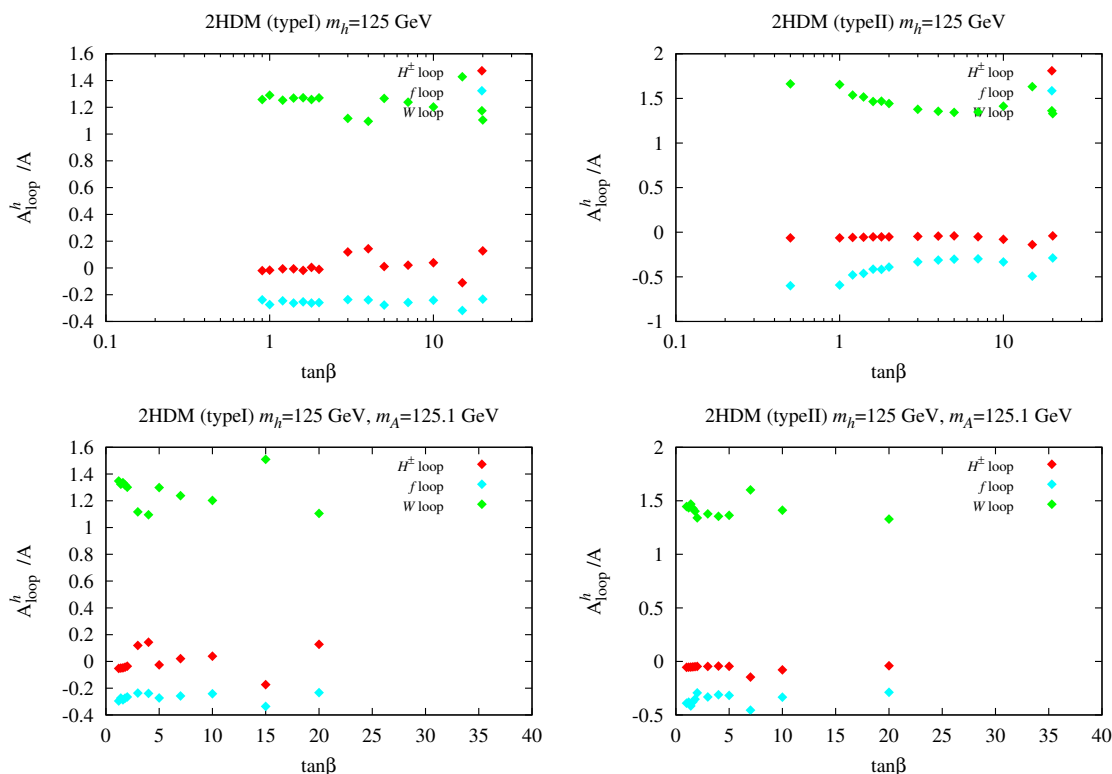


Figure 9. For the most interesting scenarios we show imaginary part of charged Higgs contributions to the $\gamma\gamma$ amplitude normalized to the imaginary part of the sum of all (fermions, W^+W^- , H^+H^-) contributions as a function of $\tan\beta$ after imposing all constraints. The parameters adopted correspond to maximal $R_{gg}^{h_i}(\gamma\gamma)$ (or an appropriate sum for degenerate cases).

all the mass parameters have been varied within what, a priori, appears to be a reasonable range, namely from a few GeV up to 1000 GeV. This is due to the fact that, for our input, the SUP conditions imply a strong constraint on m_{12}^2 that comes mainly from the requirement of keeping λ_1 small enough.

4 Conclusions

We have analyzed the Type I and Type II two-Higgs-doublet extensions of the Standard Model with regard to consistency with a significant enhancement of the gluon-fusion-induced $\gamma\gamma$ signal at the LHC at ~ 125 GeV, as seen in the ATLAS data set, but possibly not in the CMS results presented at Moriond 2013. All possible theoretical and experimental constraints have been imposed. We find that vacuum stability, unitarity and perturbativity play the key role in limiting the maximal possible enhancement which, in the most interesting scenarios, is generated by the charged Higgs loop contribution to the Higgs to two photon decay amplitude. Generically, we conclude that the Type II model allows a maximal enhancement of order of 2–3, whereas within the Type I model the maximal enhancement is limited to $\lesssim 1.3$. Moriond 2013 ATLAS results suggest an enhancement for $gg \rightarrow h \rightarrow \gamma\gamma$ of order 1.6 (but with large errors). Only Type II models can give such a large value.

However, we find that in the Type II model the parameters that give $R_{gg}^h(\gamma\gamma) \sim 1.6$ are characterized by $R_{gg}^h(ZZ) \sim (3/2)R_{gg}^h(\gamma\gamma)$, a result that is inconsistent with the ATLAS central value of $R_{gg}^h(ZZ) \sim 1.5$. Thus, the Type II model cannot describe the ATLAS data if only the h resides at 125 GeV. Similar statements apply to the case of the heavier H having a mass of 125 GeV. In contrast, the CMS data suggests values of $R_{gg}^h(\gamma\gamma) < 1$ and $R_{gg}^h(ZZ) \sim 1$, easily obtained in the Type II model context. Next, we considered Type II models with approximately degenerate Higgs bosons at 125 GeV. We found that for $1 \leq \tan\beta \leq 5$ there exist theoretically consistent parameter choices for Type II models for which $R_{gg}^{h+A}(\gamma\gamma) \sim R_{gg}^{h+A}(ZZ) \sim 1.6$, fully consistent with the ATLAS results. Unfortunately, in these cases $R_{gg}^{h+A}(\tau\tau) > 3.75$, a value far above that observed. Thus, the Type II 2HDMs cannot yield $R_{gg}^{h+A}(\gamma\gamma) \sim 1.6$ without conflicting with other observables. In short, the Type II model is unable to give a significantly enhanced $gg \rightarrow h \rightarrow \gamma\gamma$ signal while maintaining consistency with other channels.

In the case of the Type I model, the maximal $R_{gg}^h(\gamma\gamma)$ is of order of 1.3, as found if $\tan\beta = 4$ or 20. In these cases, $R_{gg}^h(ZZ)$ and $R_{gg}^h(\tau\tau)$ are of order 1. For these scenarios, the charged Higgs is light, $m_{H^\pm} = 90$ GeV. (Despite this small mass, there is no conflict with LHC data due to the fact that $BR(t \rightarrow H^+b) \sim 1/\tan^2\beta$ is small enough to be below current limits.) Thus, Type I models could provide a consistent picture if the LHC results converge to only a modest enhancement for $R_{gg}^h(\gamma\gamma) \lesssim 1.3$.

Overall, if $R_{gg}^h(\gamma\gamma)$ is definitively measured to have a value much above 1.3 while the ZZ and/or $\tau\tau$ channels show little enhancement then there is no consistent 2HDM description. One must go beyond the 2HDM to include new physics such as supersymmetry.

Acknowledgments

This work has been supported in part by US DOE grant DE-FG03-91ER40674 and by the National Science Centre (Poland) as a research project, decision no DEC-2011/01/B/ST2/00438. This work was supported by the Foundation for Polish Science International PhD Projects Programme co-financed by the EU European Regional Development Fund. JFG thanks the Galileo Galilei Institute and the LPSC Grenoble 2013 Higgs Workshop for support during the completion of this work.

Open Access. This article is distributed under the terms of the Creative Commons Attribution License which permits any use, distribution and reproduction in any medium, provided the original author(s) and source are credited.

References

- [1] ATLAS collaboration, *Observation of a new particle in the search for the Standard Model Higgs boson with the ATLAS detector at the LHC*, *Phys. Lett. B* **716** (2012) 1 [[arXiv:1207.7214](#)] [[INSPIRE](#)].
- [2] CMS collaboration, *Observation of a new boson at a mass of 125 GeV with the CMS experiment at the LHC*, *Phys. Lett. B* **716** (2012) 30 [[arXiv:1207.7235](#)] [[INSPIRE](#)].

- [3] ATLAS collaboration, *Measurements of the properties of the Higgs-like boson in the two photon decay channel with the ATLAS detector using 25 fb⁻¹ of proton-proton collision data*, [ATLAS-CONF-2013-012](#), CERN, Geneva Switzerland (2013).
- [4] CMS collaboration, *Updated measurements of the Higgs boson at 125 GeV in the two photon decay channel*, [CMS-PAS-HIG-13-001](#), in *Rencontres de Moriond*, La Thuile Italy (2013) [[INSPIRE](#)].
- [5] TEVNP (TEVATRON NEW PHENOMINA AND HIGGS WORKING GROUP), CDF and D0 collaboration, *Combined CDF and D0 search for Standard Model Higgs boson production with up to 10.0 fb⁻¹ of data*, [arXiv:1203.3774](#) [[INSPIRE](#)].
- [6] P. Ferreira, R. Santos, M. Sher and J.P. Silva, *Could the LHC two-photon signal correspond to the heavier scalar in two-Higgs-doublet models?*, *Phys. Rev. D* **85** (2012) 035020 [[arXiv:1201.0019](#)] [[INSPIRE](#)].
- [7] P. Ferreira, R. Santos, M. Sher and J.P. Silva, *Implications of the LHC two-photon signal for two-Higgs-doublet models*, *Phys. Rev. D* **85** (2012) 077703 [[arXiv:1112.3277](#)] [[INSPIRE](#)].
- [8] D.S. Alves, P.J. Fox and N.J. Weiner, *Higgs signals in a type I 2HDM or with a sister Higgs*, [arXiv:1207.5499](#) [[INSPIRE](#)].
- [9] H. Cheon and S.K. Kang, *Constraining parameter space in type-II two-Higgs doublet model in light of a 125 GeV Higgs boson*, [arXiv:1207.1083](#) [[INSPIRE](#)].
- [10] S. Chang et al., *Comprehensive study of two Higgs doublet model in light of the new boson with mass around 125 GeV*, [arXiv:1210.3439](#) [[INSPIRE](#)].
- [11] J.F. Gunion, Y. Jiang and S. Kraml, *Could two NMSSM Higgs bosons be present near 125 GeV?*, *Phys. Rev. D* **86** (2012) 071702 [[arXiv:1207.1545](#)] [[INSPIRE](#)].
- [12] P. Ferreira, H.E. Haber, R. Santos and J.P. Silva, *Mass-degenerate Higgs bosons at 125 GeV in the two-Higgs-doublet model*, [arXiv:1211.3131](#) [[INSPIRE](#)].
- [13] D. Eriksson, J. Rathsmann and O. Stal, *2HDMC: two-Higgs-doublet model calculator*, *Comput. Phys. Commun.* **181** (2010) 833 [[INSPIRE](#)].
- [14] D. Eriksson, J. Rathsmann and O. Stal, *2HDMC: two-Higgs-doublet model calculator physics and manual*, *Comput. Phys. Commun.* **181** (2010) 189 [[arXiv:0902.0851](#)] [[INSPIRE](#)].
- [15] J.F. Gunion and H.E. Haber, *The CP conserving two Higgs doublet model: the approach to the decoupling limit*, *Phys. Rev. D* **67** (2003) 075019 [[hep-ph/0207010](#)] [[INSPIRE](#)].
- [16] J.F. Gunion, H.E. Haber, G.L. Kane and S. Dawson, *The Higgs hunter's guide*, *Front. Phys.* **80** (2000) 1 [[INSPIRE](#)].
- [17] N.G. Deshpande and E. Ma, *Pattern of symmetry breaking with two Higgs doublets*, *Phys. Rev. D* **18** (1978) 2574 [[INSPIRE](#)].
- [18] M. Sher, *Electroweak Higgs potentials and vacuum stability*, *Phys. Rept.* **179** (1989) 273 [[INSPIRE](#)].
- [19] A.W. El Kaffas, W. Khater, O.M. Ogreid and P. Osland, *Consistency of the two Higgs doublet model and CP-violation in top production at the LHC*, *Nucl. Phys. B* **775** (2007) 45 [[hep-ph/0605142](#)] [[INSPIRE](#)].
- [20] I. Ginzburg and I. Ivanov, *Tree-level unitarity constraints in the most general 2HDM*, *Phys. Rev. D* **72** (2005) 115010 [[hep-ph/0508020](#)] [[INSPIRE](#)].

- [21] OPAL collaboration, G. Abbiendi et al., *Decay mode independent searches for new scalar bosons with the OPAL detector at LEP*, *Eur. Phys. J. C* **27** (2003) 311 [[hep-ex/0206022](#)] [[INSPIRE](#)].
- [22] OPAL collaboration, G. Abbiendi et al., *Flavor independent h0A0 search and two Higgs doublet model interpretation of neutral Higgs boson searches at LEP*, *Eur. Phys. J. C* **40** (2005) 317 [[hep-ex/0408097](#)] [[INSPIRE](#)].
- [23] G. Branco et al., *Theory and phenomenology of two-Higgs-doublet models*, *Phys. Rept.* **516** (2012) 1 [[arXiv:1106.0034](#)] [[INSPIRE](#)].
- [24] PARTICLE DATA GROUP collaboration, J. Beringer et al., *Review of particle physics (RPP)*, *Phys. Rev. D* **86** (2012) 010001 [[INSPIRE](#)].
- [25] S.M. Barr and A. Zee, *Electric dipole moment of the electron and of the neutron*, *Phys. Rev. Lett.* **65** (1990) 21 [*Erratum ibid.* **65** (1990) 2920] [[INSPIRE](#)].
- [26] MUON G-2 collaboration, G. Bennett et al., *Measurement of the negative muon anomalous magnetic moment to 0.7 ppm*, *Phys. Rev. Lett.* **92** (2004) 161802 [[hep-ex/0401008](#)] [[INSPIRE](#)].
- [27] F. Brummer, S. Kraml and S. Kulkarni, *Anatomy of maximal stop mixing in the MSSM*, *JHEP* **08** (2012) 089 [[arXiv:1204.5977](#)] [[INSPIRE](#)].
- [28] M. Carena, S. Gori, N.R. Shah, C.E. Wagner and L.-T. Wang, *Light stau phenomenology and the Higgs $\gamma\gamma$ rate*, *JHEP* **07** (2012) 175 [[arXiv:1205.5842](#)] [[INSPIRE](#)].
- [29] M. Aoki et al., *Light charged Higgs bosons at the LHC in 2HDMs*, *Phys. Rev. D* **84** (2011) 055028 [[arXiv:1104.3178](#)] [[INSPIRE](#)].
- [30] ATLAS collaboration, *Search for charged Higgs bosons decaying via $H^+ \rightarrow \tau\nu$ in top quark pair events using pp collision data at $\sqrt{s} = 7$ TeV with the ATLAS detector*, *JHEP* **06** (2012) 039 [[arXiv:1204.2760](#)] [[INSPIRE](#)].
- [31] CMS collaboration, *Search for a light charged Higgs boson in top quark decays in pp collisions at $\sqrt{s} = 7$ TeV*, *JHEP* **07** (2012) 143 [[arXiv:1205.5736](#)] [[INSPIRE](#)].
- [32] CMS collaboration, *Search for the Standard Model Higgs boson decaying to τ pairs in proton-proton collisions at $\sqrt{s} = 7$ and 8 TeV*, **CMS-PAS-HIG-13-004**, CERN, Geneva Switzerland (2013) [[INSPIRE](#)].
- [33] W. Altmannshofer, S. Gori and G.D. Kribs, *A minimal flavor violating 2HDM at the LHC*, *Phys. Rev. D* **86** (2012) 115009 [[arXiv:1210.2465](#)] [[INSPIRE](#)].